Journal of
Synchrotron Radiation

ISSN 0909-0495

Received 17 October 2012
Accepted 28 January 2013

Strikingly dissimilar effect of Mn and Zn dopants imposed on local structural distortion of $Ba_{0.5}K_{0.5}Fe_2As_2$ superconductor

Jie Cheng,[a] Peng Dong,[b] Wangsheng Chu,[c,d]* Wei Xu,[d] Haihu Wen,[e] Augusto Marcelli[f,g] and Ziyu Wu[c,d]*

[a]College of Science, Nanjing University of Posts and Telecommunications, Nanjing, Jiangsu 210046, People's Republic of China, [b]College of Tongda, Nanjing University of Posts and Telecommunications, Nanjing, Jiangsu 210046, People's Republic of China, [c]National Synchrotron Radiation Laboratory, University of Science and Technology of China, Hefei, Anhui 230029, People's Republic of China, [d]Beijing Synchrotron Radiation Facility, Institute of High Energy Physics, Chinese Academy of Sciences, Beijing 100049, People's Republic of China, [e]College of Physics, Nanjing University, Nanjing, Jiangsu 210093, People's Republic of China, [f]Istituto Nazionale di Fisica Nucleare, Laboratori Nazionali di Frascati, 00044 Frascati, Italy, and [g]University of Science and Technology of China, Chinese Academy of Science, Hefei 230026, People's Republic of China. E-mail: chuws@ustc.edu.cn, wuzy@ustc.edu.cn

To clarify the contrasting impurity effects of Mn and Zn dopants on the critical temperature of optimally doped $Ba_{0.5}K_{0.5}Fe_2As_2$ superconductors, extended X-ray absorption fine-structure spectroscopy was implemented at the Fe and As *K*-edge. In Mn-doped compounds a gradual deviation of the symmetric $FeAs_4$ tetrahedron and weakening of the Fe—As bond was observed. Conversely, in Zn-doped compounds the perfect $FeAs_4$ tetrahedron is maintained and the Fe—As bond is rigid. The local structural details are consistent with the development of superconductivity in these two systems, suggesting a significant role played by the topology of the $FeAs_4$ tetrahedron and rigidness of the Fe—As bond in Mn/Zn-doped $Ba_{0.5}K_{0.5}Fe_2As_2$ superconductors.

Keywords: EXAFS; local structural distortion; iron-based superconductor.

1. Introduction

The recently discovered Fe-based superconductor (FeSC) in 2008 (Kamihara *et al.*, 2008; Mizuguchi *et al.*, 2009; Rotter *et al.*, 2008) has spurred renewed interest in the mysterious superconducting mechanisms of high-T_c superconductors (Chiao, 2008; Grant, 2008). The parent phases of FeSC are 'bad metals' accompanied by antiferromagnetism, and the superconductivity occurs upon chemical doping or pressure. For instance, the superconductivity of the first reported FeSC, $LaFeAsO_{1-x}F_x$, is attained by the replacement of O atoms by F (electron-doping) (Kamihara *et al.*, 2008); with K-doping the $Ba_{1-x}K_xFe_2As_2$ system can exhibit its maximum critical temperature (T_c) of T_c = 38 K (hole-doping) (Rotter *et al.*, 2008); meanwhile, the T_c of $FeSe_{1-x}$ is extremely sensitive to applied external pressure, rising from 13.5 K at ambient pressure to 27 K at 14.8 GPa (Margadonna *et al.*, 2008). Here, strikingly different from the cuprates in which doping at the Cu site would suppress superconductivity, the substitution of Co/Ni or rather the isovalent Ru for the Fe-site doped FeSC induces superconductivity (Kim *et al.*, 2011; Sefat *et al.*, 2008; Wang *et al.*, 2010), while to date the superconducting phase has not been observed by Cr/Mn/Cu doping (Canfield *et al.*, 2009; Kim *et al.*, 2010; Sefat *et al.*, 2009). In analogy to cuprates, the phase diagram of FeSC displays the competition between antiferromagnetism and superconductivity, and the onset of the T_c always displays a dome-like shape (Ahilan *et al.*, 2009; Chen *et al.*, 2009; Gooch *et al.*, 2008; Kamihara *et al.*, 2008). That is, in the lightly doped region T_c increases rapidly until it reaches a critical doping concentration (*i.e.* the so-called optimal doping level); however, the reduction of T_c emerges in heavily doped regimes. In the case of the $Ba_{1-x}K_xFe_2As_2$ system, the K optimal doping concentration is $x \simeq 0.5$ (Chen *et al.*, 2009).

To better understand the superconducting properties of FeSC, researchers have also resorted to co-doped systems (Canfield *et al.*, 2009; Luo *et al.*, 2011; Suzuki *et al.*, 2010). According to Anderson's theorem (Anderson, 1959), non-magnetic impurities are regarded as important probes for the pairing symmetry of high-T_c superconductors. As a consequence, several studies regarding the Zn impurity effect on the superconductivity of FeSC have been reported (Guo *et al.*, 2010; Li *et al.*, 2011, 2010*a*,*b*; Kitagawa *et al.*, 2011). Cheng *et al.* (2010*a*) found that in optimally doped $Ba_{0.5}K_{0.5}Fe_2As_2$ superconductor the superconducting temperature T_c is drastically reduced by a Mn impurity whereas it is not sensitive

to non-magnetic Zn impurities, which was interpreted as a consequence of the different magnetic scattering strengths of Mn and Zn dopants. Until now a satisfactory understanding of the superconducting mechanism has far from been achieved. Considering the intimate relationship between superconductivity and the atomic structure of high-T_c superconductors (Lee *et al.*, 2008; Mizuguchi *et al.*, 2010), it is desirable to identify local lattice structural distortions induced by impurities, thus illustrating the mechanism of different impurity effects between Mn and Zn dopants on the optimally doped $Ba_{0.5}K_{0.5}Fe_2As_2$ superconductor (Cheng *et al.*, 2010*a*).

Conventional techniques such as X-ray diffraction can only provide the average structural information, and is not sensitive to the local structural distortions induced by different dopants. Synchrotron-radiation-based extended X-ray absorption fine structure (EXAFS), however, is a powerful element-selective local structural probe and has been effective in investigating the local lattice structure of FeSC (Cheng *et al.*, 2010*b*; Granado *et al.*, 2011) and other related high-T_c superconductors such as cuprates (Zhang & Oyanagi, 2009). Meanwhile, by applying EXAFS in a temperature-dependent experiment, useful lattice dynamic information, such as the force constant of the atomic bond (Cheng *et al.*, 2010*b*; Joseph *et al.*, 2011), can also be quantitatively estimated. In this contribution we report a quantitative estimation of local structural distortions induced by Mn and Zn impurities in $Ba_{0.5}K_{0.5}Fe_2As_2$ compounds, through a comprehensive analysis of temperature-dependent EXAFS at the Fe and As *K*-edge.

2. Experiments

The Mn-doped and Zn-doped polycrystalline compounds $Ba_{0.5}K_{0.5}(Fe_{1-x}TM_x)_2As_2$ (TM = Mn, x = 0, 0.02, 0.04, 0.08; TM = Zn, x = 0, 0.08) were synthesized by conventional solid-state reaction method (Cheng *et al.*, 2010*a*). Samples were ground into fine powders and then brushed onto tapes that were stacked to give approximately one X-ray-absorption length at their corresponding absorption edges. Fe and As *K*-edge EXAFS spectra of $Ba_{0.5}K_{0.5}(Fe_{1-x}TM_x)_2As_2$ were recorded at room temperature in transmission mode at the 1W2B beamline of the Beijing Synchrotron Radiation Facility (BSRF), running at an electron energy of 2.5 GeV with a maximum current of ~250 mA. The flux on the sample of beamline 1W2B is 10^{12} photons s^{-1} at 9 keV, and the energy resolution is better than 4×10^{-4} at 9 keV. Moreover, the temperature-dependent Fe and As *K*-edge EXAFS experiments on $Ba_{0.5}K_{0.5}Fe_2As_2$ and $Ba_{0.5}K_{0.5}(Fe_{1-x}TM_x)_2As_2$ (TM = Mn and Zn, x = 0.08) were carried out to an accuracy of ±1 K using a Si(111) double-crystal monochromator at the 1W1B beamline at BSRF. The EXAFS spectra were analyzed using *IFEFFIT* (Newville, 2001); for the data fitting the backscattering amplitudes and total phase shifts were calculated using the $BaFe_2As_2$ model cluster of type $ThCr_2Si_2$ with the *FEFF8.2* code (Ankudinov *et al.*, 1998).

3. Results and discussions

Fourier transforms (FTs) of the EXAFS spectra of the Mn-doped and Zn-doped $Ba_{0.5}K_{0.5}Fe_2As_2$ samples are plotted in Fig. 1. It should be pointed out that the k-range for the Fourier transform was 2.4–12.1 $Å^{-1}$ for the As-edge and 2.5–12.2 $Å^{-1}$ for the Fe-edge. For As-edge EXAFS, the first peak in the radial distribution function (RDF) results from the contribution of the four nearest Fe atoms. For Fe-edge EXAFS the first peak of the RDF is a superposition of two subshells including Fe—As and Fe—Fe bonds. It can be found that, despite the lower intensity, the overall RDF of Mn/Zn-doped compounds is similar to that of $Ba_{0.5}K_{0.5}Fe_2As_2$, indicating that Mn/Zn doping finely modulates the local structure of the FeAs superconducting layer, which was believed to be intimately related to the superconductivity of FeSC (Cheng *et al.*, 2010*b*).

To estimate the Mn/Zn doping effect quantitatively, we performed structural fittings on the first peak of both As and Fe *K*-edge EXAFS spectra, which were isolated from the FTs by a rectangular window. The range in k-space was 2.4–12.1 $Å^{-1}$ and that in R-space was 1.4–2.6 Å for the As *K*-edge;

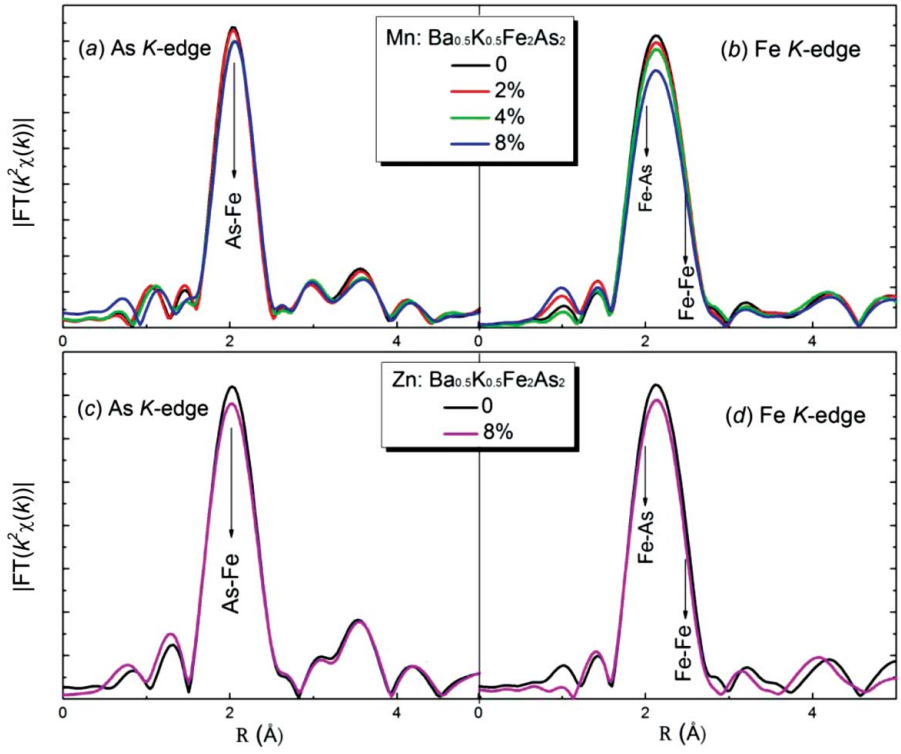

Figure 1
Comparison of the Fourier transforms of the $k^2\chi(k)$ EXAFS signals for $Ba_{0.5}K_{0.5}(Fe_{1-x}TM_x)_2As_2$ compounds at the As *K*-edge [panels (*a*) and (*c*)] and Fe *K*-edge [panels (*b*) and (*d*)].

for the Fe K-edge the k-range was 2.5–12.2 Å^{-1} and the R-range was 1.4–2.9 Å. During fitting, the Mn/Zn—As and Mn/Zn—Fe contributions are not considered, owing to the low doping level of Mn/Zn. The number of independent parameters which could be determined by EXAFS is limited by the number of independent data points $N_{\rm ind} \simeq (2\Delta k \Delta R)/\pi$, where Δk and ΔR are, respectively, the ranges of the fit in the k- and R-space. Thus $N_{\rm ind}$ is 7 (Δk = 9.7 Å^{-1}, ΔR = 1.2 Å) for the As—Fe shell at the As-edge, and $N_{\rm ind}$ is 9 (Δk = 9.7 Å^{-1}, ΔR = 1.5 Å) for the Fe—As and the Fe—Fe shells at the Fe-edge, sufficient to obtain all parameters. At first we fit the As-edge, fixing the As—Fe coordination number and obtaining the As—Fe distance and the Debye–Waller factor (DWF) $\sigma^2_{\rm As-Fe}$. For the Fe-edge we applied two-shells fitting. To reduce fit variables, the coordination numbers of Fe—As and Fe—Fe, the distance of Fe—As and the DWF $\sigma^2_{\rm Fe-As}$ (the same as $\sigma^2_{\rm As-Fe}$ obtained from the As-edge fitting) were fixed, leaving the other parameters free. The fitting results are summarized in Figs. 2 and 3. Owing to the lattice mismatch, Mn doping induces a gradual increase of the Fe—As distance and a reduction in the Fe—Fe bond length. Both Fe—As and Fe—Fe distances are almost independent of the Zn impurity, confirming the structural stability of the FeAs layers.

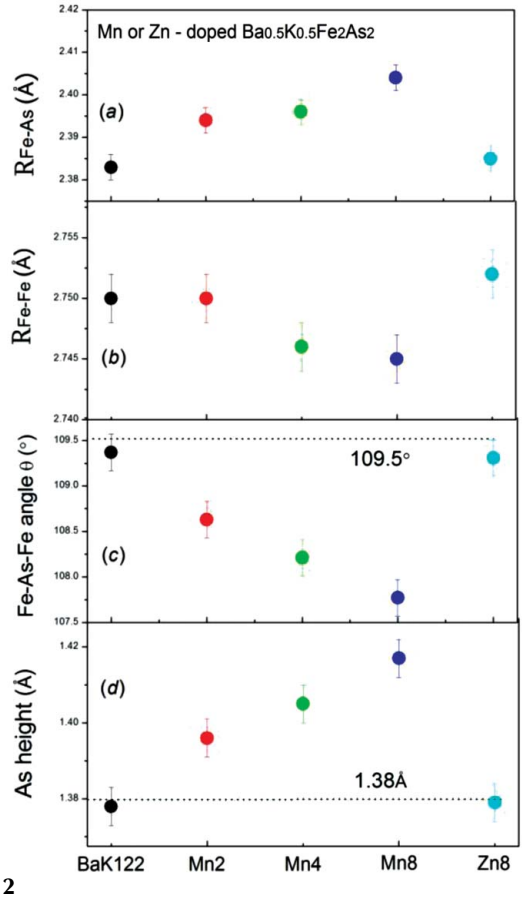

Figure 2
Fe—As distance (*a*), Fe—Fe distance (*b*), Fe—As—Fe angle (*c*) and As height (*d*) for $Ba_{0.5}K_{0.5}(Fe_{1-x}TM_x)_2As_2$ compounds as a function of Mn/Zn doping concentration. For the sake of simplicity, the $Ba_{0.5}K_{0.5}Fe_2As_2$ sample is labeled as BaK122, while Mn2, Mn4, Mn8 and Zn8 are, respectively, the abbreviations of $Ba_{0.5}K_{0.5}(Fe_{1-x}TM_x)_2As_2$ compounds with TM = Mn, x = 0.02, 0.04, 0.08 and TM = Zn, x = 0.08.

The superconductivity in FeSC is known to be extremely sensitive to the structural topology of the $FeAs_4$ tetrahedron and As height from the Fe layer (Lee *et al.*, 2008; Mizuguchi *et al.*, 2010). Many statistical investigations claim that the highest T_c is attained as the $FeAs_4$ coordination approaches a regular tetrahedron with an Fe—As—Fe angle of about 109.47° (Lee *et al.*, 2008). Meanwhile, the optimal value of the As height is about 1.38 Å for the best superconducting property (Mizuguchi *et al.*, 2010). According to the above findings, the Fe—As—Fe angle and the As height are important structural parameters; therefore we evaluated the Fe—As—Fe bond angle and As height as a function of Mn/Zn doping. The result is shown in Figs. 2(*c*) and 2(*d*). With the doping concentration of Mn increasing, the Fe—As—Fe bond angle gradually deviates from a perfect tetrahedron, accompanied by the elevating distance of As from the Fe layer. It was found that small structural changes in the $FeAs_4$ tetrahedron and As height can affect the band-filling/Fermi-surface nesting and thus the superconducting gap (Kuroki *et al.*, 2009). Accordingly, the suppression of superconductivity in Mn-doped samples can be attributed to local structural modulations in $FeAs_4$ tetrahedra. In contrast, the $FeAs_4$ tetrahedra are maintained regularly in the Zn-doped samples with the optimal As height. It is once more proved that structural modification of FeAs layers, especially the topology of the $FeAs_4$ tetrahedron, plays a crucial role in the superconductivity of FeSC.

The doping mechanism may also be investigated by studying the behavior of the DWF, σ^2, measuring the mean square relative displacement (MSRD) of the photon absorber–backscatterer pairs. In Fig. 3 we plot the MSRDs of Fe—As and Fe—Fe pairs as a function of Mn/Zn doping concentration. The data show that in the presence of Mn/Zn impurity the DWFs of both Fe—As and Fe—Fe pairs exhibit a clear increase.

The DWF of each atom pair is the sum of two contributions, *i.e.* $\sigma^2 = \sigma^2_0 + \sigma^2_{\rm vib}$. The term σ^2_0 is temperature independent and associated with the static disorder. $\sigma^2_{\rm vib}$ originates from thermal vibrations and can be described by the Einstein model (Knapp *et al.*, 1985) as $\sigma^2_{\rm vib} = (\hbar^2/2k_B\mu T_E)\coth(T_E/2T)$. In this equation $\hbar$ is the Plank constant, k_B is the Boltzmann constant, μ is the reduced mass of the atom pair, and T is the temperature. The Einstein temperature $T_E = (\hbar/k_B)\omega_E$ is proportional to the square root of the force constant for a bond; therefore this value can be utilized to estimate and compare the stiffness of different bonds.

In order to recognize whether the increased disorders of the Fe—As and Fe—Fe pairs *versus* Mn/Zn doping are static or dynamic, temperature-dependent EXAFS was performed. Fig. 4 displays the Fe—As and Fe—Fe DWFs as a function of temperature for the $Ba_{0.5}K_{0.5}Fe_2As_2$ and 8% Mn/Zn-doped compounds, and the simulations are implemented by the classical Einstein model (Cheng *et al.*, 2010*b*). It can be seen that all the Fe—As and Fe—Fe DWFs show almost identical temperature dependence for these samples. Although the temperature dependence looks similar, there seems to be a clear discrepancy in the Einstein temperature T_E. For the Fe—

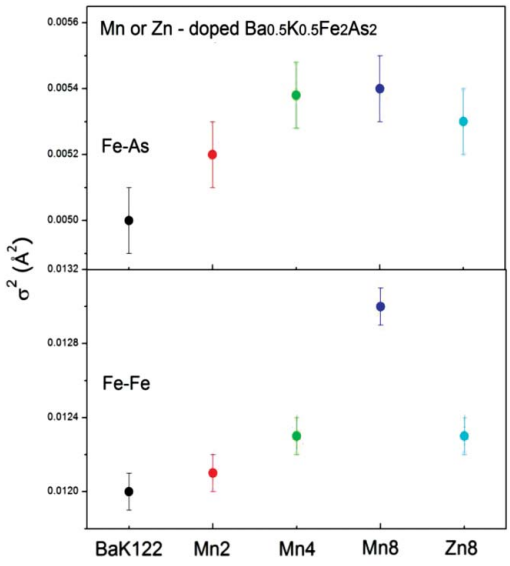

Figure 3
Mean square relative displacement (MSRD) of the Fe—As and Fe—Fe pairs for $Ba_{0.5}K_{0.5}(Fe_{1-x}TM_x)_2As_2$ compounds as a function of Mn/Zn doping concentration.

Fe bond, the T_E values for $Ba_{0.5}K_{0.5}Fe_2As_2$, 8% Mn-doped and 8% Zn-doped $Ba_{0.5}K_{0.5}Fe_2As_2$ compounds are 228.7 K, 220.2 K and 205.8 K, respectively. Therefore the Fe—Fe bond seems to become softer in the Mn/Zn-doped system, accompanied by a weakening of the Fe—Fe interactions. On the other hand, Mn/Zn dopants also affect the DWFs of the Fe—As pair significantly. The T_E value of the Fe—As bond for $Ba_{0.5}K_{0.5}Fe_2As_2$ is about 352.3 K; it becomes 349.7 K for the 8% Mn-doped compound, while Zn doping yields a higher T_E of 362.7 K, clearly indicating the contrastingly different doping effects on the Fe—As bond between Mn and Zn impurities.

A systematic variation of the T_E values of the Fe—As bond for the ReFeAsO (Re = La, Sm, Nd) compounds was reported by Joseph *et al.* (2010), revealing that a harder Fe—As bond is favorable for the higher T_c in oxypnictide systems. Similarly, here for the $Ba_{0.5}K_{0.5}Fe_2As_2$-based system, an enhanced Fe—As bond can be beneficial for Zn doping, while the weakening of that bond may be intimately associated with a gradual suppression of the superconductivity in Mn-doped compounds.

4. Conclusion

We compared the local structure of the optimally doped $Ba_{0.5}K_{0.5}Fe_2As_2$ superconductor and Mn/Zn-doped $Ba_{0.5}K_{0.5}Fe_2As_2$ compounds by employing temperature-dependent EXAFS at the As and Fe *K*-edge. For Mn-doped samples in which superconductivity is remarkably suppressed, a noticeable distortion of the regular $FeAs_4$ tetrahedron is observed. By contrast, in Zn-doped samples the $FeAs_4$ tetrahedron remains rigid and regular. On the other hand, with doping the Fe—Fe bond becomes softer in both cases while the Fe—As bond is more rigid in the Zn-doped system than in the Mn-doped system, as suggested by the Einstein temperature of the bonds.

The superconductivity is known to be closely related to the regular configuration of the $FeAs_4$ tetrahedron which can directly modulate the band-filling/Fermi-surface nesting and also the superconducting gap for FeSC. Therefore, we propose that the strikingly dissimilar impurity effects on T_c originate primarily on the local structural distortions which are more pronounced in the Mn-doped system than in the Zn-doped system. This new scenario may compensate for the previous magnetic scattering description, thus offering new insights on the interplay of atomic spin and charge in iron-based superconductors.

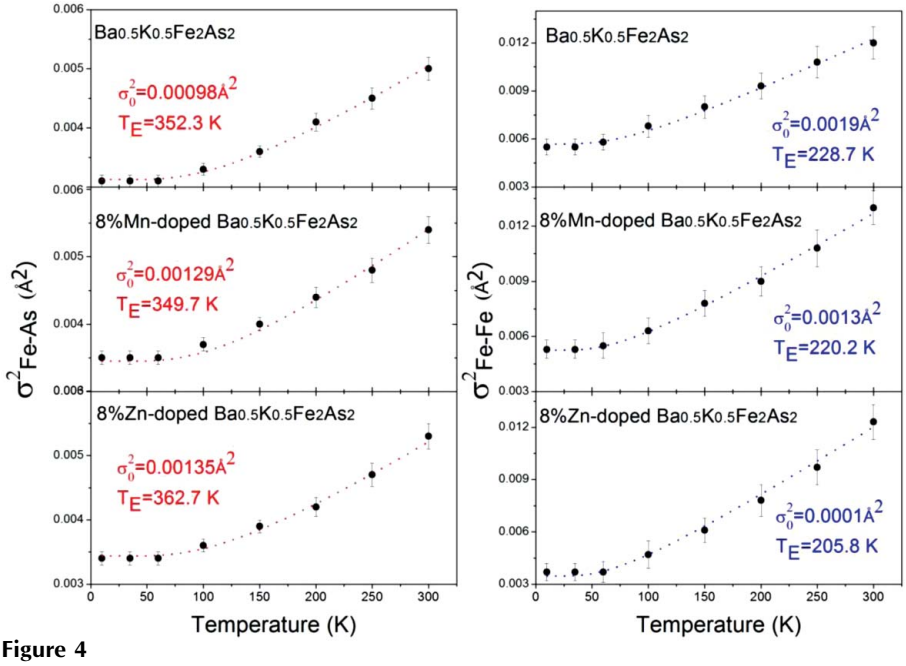

Figure 4
Temperature-dependent MSRD of the Fe—As and Fe—Fe pairs (symbols) for $Ba_{0.5}K_{0.5}(Fe_{1-x}TM_x)_2As_2$ compounds as a function of Mn/Zn doping concentrations and their simulations using the classical Einstein model (dotted lines).

This work was partly supported by the National Outstanding Youth Fund (10125523), the Knowledge Innovation Program of the Chinese Academy of Sciences (KJCX2-YW-N42), the National Natural Science Foundation of China (11179023) and the Fundamental Research Funds for the Central Universities (WK2310000019).

References

Ahilan, K., Ning, F., Imai, T., Sefat, A., McGuire, M., Sales, B. & Mandrus, D. (2009). *Phys. Rev. B*, **79**, 214520.
Anderson, P. (1959). *J. Phys. Chem. Solids*, **11**, 26–30.

Ankudinov, A. L., Ravel, B., Rehr, J. J. & Conradson, S. D. (1998). *Phys. Rev. B*, **58**, 7565.
Canfield, P., Bud'ko, S., Ni, N., Yan, J. & Kracher, A. (2009). *Phys. Rev. B*, **80**, 060501.
Chen, H., Ren, Y., Qiu, Y., Bao, W., Liu, R. H., Wu, G., Wu, T., Xie, Y. L., Wang, X. F., Huang, Q. & Chen, X. H. (2009). *Europhys. Lett.* **85**, 17006.
Cheng, J., Chu, W. S., Wu, G., Zhao, H. F., Xu, W., Zhou, J., Zhang, L. J., Chen, X. H. & Wu, Z. Y. (2010*b*). *J. Synchrotron Rad.* **17**, 730–736.
Cheng, P., Shen, B., Hu, J. & Wen, H. (2010*a*). *Phys. Rev. B*, **81**, 174529.
Chiao, M. (2008). *Nat. Phys.* **4**, 446.
Gooch, M., Lv, B., Lorenz, B., Guloy, A. M. & Chu, C.-W. (2008). *Phys. Rev. B*, **78**, 180508.
Granado, E., Mendonca-Ferreira, L., Garcia, F., Azevedo, G. de M., Fabbris, G., Bittar, E. M., Adriano, C., Garitezi, T. M., Rosa, P. F. S., Bufaical, L. F., Avila, M. A., Terashita, H. & Pagliuso, P. G. (2011). *Phys. Rev. B*, **83**, 184508.
Grant, P. M. (2008). *Nature (London)*, **453**, 1000–1001.
Guo, Y. F., Shi, Y. G., Yu, S., Belik, A. A., Matsushita, Y., Tanaka, M., Katsuya, Y., Kobayashi, K., Nowik, I., Felner, I., Awana, V. P. S., Yamaura, K. & Takayama-Muromachi, E. (2010). *Phys. Rev. B*, **82**, 054506.
Joseph, B., Iadecola, A., Malavasi, L. & Saini, N. L. (2011). *J. Phys. Condens. Matter*, **23**, 265701.
Joseph, B., Iadecola, A., Puri, A., Simonelli, L., Mizuguchi, Y., Takano, Y. & Saini, N. L. (2010). *Phys. Rev. B*, **82**, 020502.
Kamihara, Y., Watanabe, T., Hirano, M. & Hosono, H. (2008). *J. Am. Chem. Soc.* **130**, 3296–3297.
Kim, J. S., Khim, S., Kim, H. J., Eom, M. J., Law, J. M., Kremer, R. K., Shim, J. H. & Kim, K. H. (2010). *Phys. Rev. B*, **82**, 024510.
Kim, M. G., Pratt, D. K., Rustan, G. E., Tian, W., Zarestky, J. L., Thaler, A., Bud'ko, S. L., Canfield, P. C., McQueeney, R. J., Kreyssig, A. & Goldman, A. I. (2011). *Phys. Rev. B*, **83**, 054514.
Kitagawa, S., Nakai, Y., Iye, T., Ishida, K., Guo, Y. F., Shi, Y. G., Yamaura, K. & Takayama-Muromachi, E. (2011). *Phys. Rev. B*, **83**, 180501.
Knapp, G., Pan, H. & Tranquada, J. (1985). *Phys. Rev. B*, **32**, 2006–2009.
Kuroki, K., Usui, H., Onari, S., Arita, R. & Aoki, H. (2009). *Phys. Rev. B*, **79**, 224511.
Lee, C. H., Iyo, A., Eisaki, H., Kito, H., Fernandez-Diaz, M. T., Ito, T., Kihou, K., Gooch, M., Lv, B., Lorenz, B., Guloy, A. M. & Chu, C.-W. (2008). *Phys. Rev. B*, **78**, 180508.
Li, J., Guo, Y., Zhang, S., Yu, S., Tsujimoto, Y., Kontani, H., Yamaura, K. & Takayama-Muromachi, E. (2011). *Phys. Rev. B*, **84**, 020513.
Li, Y. K., Lin, X., Tao, Q., Wang, C., Zhou, T., Li, L. J., Wang, Q. B., He, M., Cao, G. H. & Xu, Z.-A. (2010a). *New J. Phys.* **12**, 053008.
Li, Y., Tong, J., Tao, Q., Feng, C., Cao, G., Chen, W., Zhang, F. & Xu, Z. (2010b). *New J. Phys.* **12**, 083008.
Luo, Y., Han, H., Jiang, S., Lin, X., Li, Y., Dai, J., Cao, G. & Xu, Z. (2011). *Phys. Rev. B*, **83**, 054501.
Margadonna, S., Takabayashi, Y., McDonald, M. T., Kasperkiewicz, K., Mizuguchi, Y., Takano, Y., Fitch, A. N., Suard, E. & Prassides, K. (2008). *Chem. Commun.* pp. 5607–5609.
Mizuguchi, Y., Hara, Y., Deguchi, K., Tsuda, S., Yamaguchi, T., Takeda, K., Kotegawa, H., Tou, H. & Takano, Y. (2010). *Supercond. Sci. Tech.* **23**, 054013.
Mizuguchi, Y., Tomioka, F., Tsuda, S., Yamaguchi, T. & Takano, Y. (2009). *Appl. Phys. Lett.* **94**, 012503.
Newville, M. (2001). *J. Synchrotron Rad.* **8**, 322–324.
Rotter, M., Tegel, M. & Johrendt, D. (2008). *Phys. Rev. Lett.* **101**, 107006.
Sefat, A. S., Jin, R., McGuire, M. A., Sales, B. C., Singh, D. J. & Mandrus, D. (2008). *Phys. Rev. Lett.* **101**, 117004.
Sefat, A., Singh, D., VanBebber, L., Mozharivskyj, Y., McGuire, M., Jin, R., Sales, B., Keppens, V. & Mandrus, D. (2009). *Phys. Rev. B*, **79**, 224524.
Suzuki, S., Ohgushi, K., Kiuchi, Y. & Ueda, Y. (2010). *Phys. Rev. B*, **82**, 184510.
Wang, M., Luo, H., Zhao, J., Zhang, C., Wang, M., Marty, K., Chi, S., Lynn, J. W., Schneidewind, A., Li, S. & Dai, P. (2010). *Phys. Rev. B*, **81**, 174524.
Zhang, C. & Oyanagi, H. (2009). *Phys. Rev. B*, **79**, 064521.